# Experimental and theoretical study of deuteron-proton elastic scattering for proton kinetic energies between $T_p = 882.2$ MeV and $T_p = 918.3$ MeV

**Editorial team:**, C. Fritzsch[a,*], M. N. Platonova[b], V. I. Kukulin[b], C. Wilkin[c]

[a] *Institut für Kernphysik, Westfälische Wilhelms-Universität Münster, Wilhelm-Klemm-Str. 9, 48149 Münster, Germany*
[b] *Skobeltsyn Institute of Nuclear Physics, Lomonosov Moscow State University, Leninskie Gory 1/2, 119991 Moscow, Russia*
[c] *Physics and Astronomy Department, UCL, Gower Street, London WC1E 6BT, United Kingdom*

## Abstract

New precise unpolarised differential cross sections of deuteron-proton elastic scattering have been measured at 16 different deuteron beam momenta between $p_d = 3120.17$ MeV/$c$ and $p_d = 3204.16$ MeV/$c$ at the COoler SYnchrotron COSY of the Forschungszentrum Jülich. The data, which were taken using the magnetic spectrometer ANKE, cover the equivalent range in proton kinetic energies from $T_p = 882.2$ MeV to $T_p = 918.3$ MeV. The experimental results are analysed theoretically using the Glauber diffraction model with accurate nucleon-nucleon input. The theoretical cross section at $T_p = 900$ MeV agrees very well with the experimental one at low momentum transfers $|t| < 0.2$ (GeV/$c$)$^2$.

*Keywords:* deuteron-proton elastic scattering, Glauber model

## 1. Introduction

Deuteron-proton elastic scattering is extensively used in the study of, e.g., meson production mechanisms in few nucleon systems at intermediate energies. For such experiments $dp$ elastic scattering is well suited for normalisation purposes, due to its high cross section over a large momentum transfer range (cf. Fig. 1). Previous work on meson production, e.g., Refs. [1, 2, 3], used the existing database [4, 5, 6, 7, 8] for data normalisation, assuming that for low momentum transfers, i.e., $|t| < 0.4$ (GeV/$c$)$^2$, the differential cross section as a function of $t$ is independent of the beam momentum in the proton kinetic energy range between $T_p = 641$ MeV and $T_p = 1000$ MeV.

In contrast to the database at smaller momentum transfers $|t| < 0.1$ (GeV/$c$)$^2$, that at larger $|t|$ is much poorer. High-precision data from the ANKE spectrometer, using a deuteron beam and a hydrogen target, allows further study of the behaviour of the unpolarised differential cross sections. This enlarges the database in the momentum transfer range $0.08 < |t| < 0.26$ (GeV/$c$)$^2$ at deuteron momenta that correspond to proton energies between $T_p = 882.2$ MeV and $T_p = 918.3$ MeV.

On the theoretical side, $pd$ elastic scattering in the GeV energy region has usually been analysed in terms of the Glauber diffraction model (or its various extensions), which is a high-energy and low-momentum-transfer approximation to the exact multiple-scattering series for the hadron-nucleus scattering amplitude. The original Glauber model [9], where spin degrees of freedom were neglected (or included only partially), has been refined [10, 11] by taking fully into account the spin structure of colliding particles, i.e., the spin-dependent $NN$ amplitudes and the $D$-wave component of the deuteron wave function, and also the double-charge-exchange process $p + d \to n + (pp) \to p + d$. In addition, while the majority of previous calculations made within the Glauber model employed simple parameterisations for the forward $NN$ amplitudes, the refined model [10, 11] suggests using accurate $NN$ amplitudes, based on modern $NN$ partial-wave analysis (PWA). By using the $NN$ PWA of the George Washington University SAID group (SAID) [12], the model has been shown to describe small-angle $pd$ differential cross sections and also the more sensitive polari-

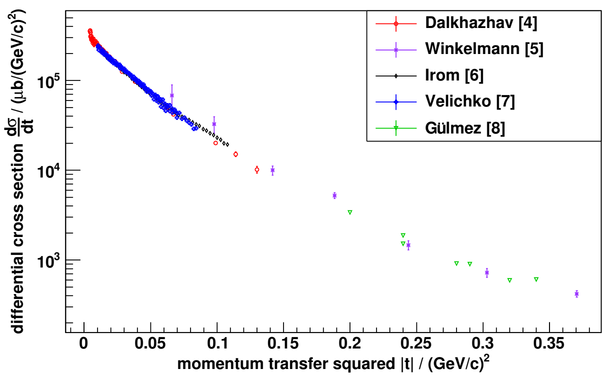


Figure 1: Unpolarised differential cross sections of $dp$ elastic scattering plotted as a function of the momentum transfer squared $-t$ for different data sets [4, 5, 6, 7, 8].

*Corresponding author
*Email address:* c.fritzsch@uni-muenster.de (C. Fritzsch)

sation observables very well in the energy range $T_p = 200-1000$ MeV [10]. The refined Glauber model therefore seems ideally suited for the description of the experimental data presented here. On the other hand, the new high-precision data can provide a precise test for applicability of the Glauber model.

The SAID group has recently published an updated $NN$ PWA solution [13], which incorporates the new COSY-ANKE data on the near-forward cross section [14] and analysing power $A_y$ [15] in $pp$ elastic scattering, as well as the recent COSY-WASA $A_y$ data [16] in $np$ elastic scattering. We can therefore re-examine the predictions of the refined Glauber model obtained with the use of the previous PWA solution of 2007 [12]. By performing calculations at various incident energies, we can also test the widely-used assumption of energy independence of the $pd$ elastic differential cross section at low momentum transfers.

## 2. Experimental Setup

The data were taken with the magnetic spectrometer ANKE [17] (cf. Fig. 2 for a schematic representation of the setup), which is part of an internal fixed-target experiment located at the COoler SYnchrotron – COSY of the Forschungszentrum Jülich. One of the main components of ANKE is the magnetic system, with its three dipole magnets D1–D3. The accelerated beam of unpolarized deuterons is deflected by the first dipole magnet D1 (cf. Fig. 2) into the target chamber, where the beam interacts with the internal hydrogen cluster-jet target [18].

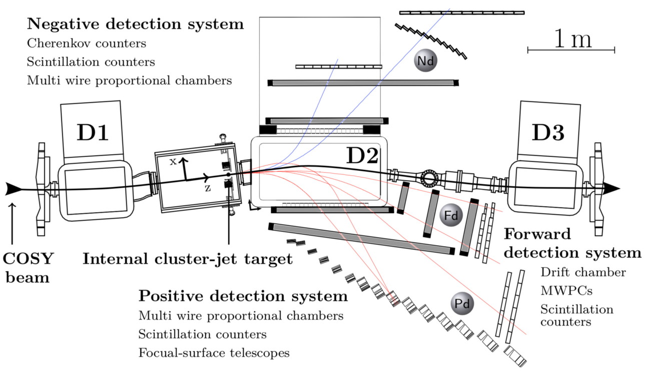


Figure 2: Schematic view of the ANKE magnetic spectrometer. It mainly consists of three dipole magnets, an internal hydrogen cluster jet-target and three detection systems (Pd-, Nd- and Fd-system). The red lines represent possible tracks of positively charged particles and the blue lines of negatively charged particles.

The second dipole magnet D2 separates the ejectiles by their electric charge into three different detection systems. The deuterons associated with $dp$ elastic scattering are deflected by D2 into the Forward (Fd) detection system, which was the only element used in this experiment. The Fd was designed and installed near the beam pipe to detect heavy or fast particles. Beam particles not interacting with the internal target are deflected by the dipole magnets D2 and D3 back onto the nominal ring orbit. A special feature of this magnetic spectrometer is the moveable D2 magnet, which can be shifted perpendicular to the beam line. It is thus possible to optimise the geometrical acceptance of the detection system for each reaction that one would like to investigate.

The deuteron beam momentum range from 3120.17 MeV/$c$ to 3204.16 MeV/$c$ was divided into 16 different fixed beam momenta (cf. Table 1, originally for the determination of the $\eta$ meson mass [19]) using the supercycle mode of COSY. In each supercycle it is possible to alternate between up to seven different beam settings, each with a cycle length of 206 s. The value of $\Delta p_{\text{beam}}/p_{\text{beam}} < 6 \times 10^{-5}$ was determined using the spin depolarisation technique [20].

Table 1: Beam momenta $p_d$ for each supercycle and flattop in MeV/$c$.

| | FT1 | FT2 | FT3 | FT4 | FT5 | FT6 | FT7 |
|---|---|---|---|---|---|---|---|
| SC1 | 3120.17 | 3146.41 | 3148.45 | 3152.45 | 3158.71 | 3168.05 | 3177.51 |
| SC2 | 3120.17 | 3147.35 | 3150.42 | 3154.49 | 3162.78 | 3172.15 | 3184.87 |
| SC3 | | | | 3157.48 | 3160.62 | | 3204.16 |

## 3. Event Selection and Analysis

As described above, deuterons originating from $dp$ elastic scattering are deflected by D2 into the Forward detection system, which consists of one multiwire drift chamber as well as two multiwire proportional chambers for track reconstruction. In addition, two scintillator hodoscopes, comprised of eight vertically aligned scintillator strips for the first and nine for the second hodoscope, are used for particle identification using the energy-loss information and time-of-flight measurements.

During the data taking a specific hardware trigger was included, which required two coincident scintillator signals, one in each of the two Fd hodoscopes. Due to the cross section for $dp$ elastic scattering being very large, this hardware trigger is equipped with a pre-scaling factor of 1024 to reduce the dead time of the data acquisition system.

On account of the small momentum transfer to the target proton, the forward-going deuterons, whose tracks are reconstructed in the Forward detection system, have momenta close to that of the beam. Since only deuterons from elastic scattering have such a high momentum, the reaction can be identified with no physical background from meson production. Reconstructed particles with a momentum $p$ below about $p/p_d \approx 0.913$ are discarded to obtain a better signal-to-noise ratio.

In order to avoid uncertainties caused by possible inhomogeneities of the magnetic field at the edges of the D2 magnet, an additional cut in the $y$ hit position (with $y$

being the axis perpendicular to the COSY plane) of the first multi-wire proportional chamber is required. Events with $|y_{\rm hit}| > 105$ mm are discarded.

For $dp$ elastic scattering the geometrical acceptance of the ANKE magnetic spectrometer is limited to $0.06 < |t| < 0.31$ (GeV/$c$)$^2$. However, to avoid systematic edge effects, only events in the region $0.08 < |t| < 0.26$ (GeV/$c$)$^2$ were analysed, with a bin width of $\Delta t = 0.01$ (GeV/$c$)$^2$. The missing-mass analysis of Fig. 3 shows a prominent signal at the proton mass sitting on top of a very small and seemingly constant background. A Gaussian fit to the peak was used to define its position and width and the region outside the $\pm 3\sigma$ region was used to fit a constant background. After subtracting this, the missing-mass spectra are integrated to obtain the number of $dp$ elastic scattering events for each of the 18 momentum transfer bins at all 16 different beam momenta.

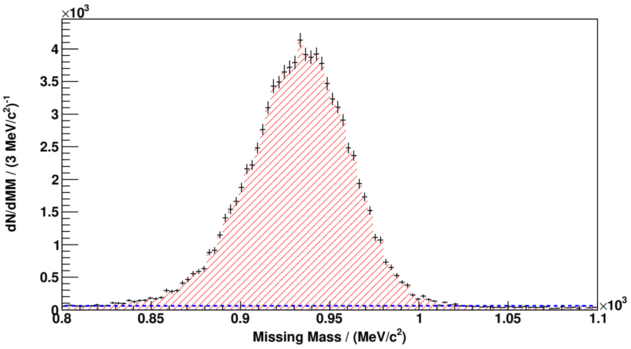


Figure 3: Missing-mass spectrum of the $dp \to dX$ reaction at $p_d =$ 3120.17 MeV/$c$ for $0.08 < |t| < 0.09$ (GeV/$c$)$^2$. The blue dashed line represents a constant background fit to the spectrum, excluding the $\pm 3\sigma$ region around the peak.

The detector acceptance, which drops from 15% to 7% with increasing momentum transfer. was determined using Monte Carlo simulations. These simulations have to fulfil the same software cut criteria as the data, so that the acceptance-corrected count yield can be determined for each beam momentum setting. The resulting differential cross sections are presented in Sec. 5.

## 4. Theoretical calculation

The theoretical calculation of the $pd$ elastic scattering cross section was performed at four incident proton energies $T_p = 800$, 900, 950 and 1000 MeV within the refined Glauber model [10, 11]. The differential cross section is related to the amplitude $M$ as

$$\mathrm{d}\sigma/\mathrm{d}t = \tfrac{1}{6}\mathrm{Sp}\left(MM^{+}\right). \tag{1}$$

The $pd$ amplitude $M$ in the Glauber approach contains two terms corresponding to single and double scattering of the projectile with the nucleons in the deuteron. These terms are expressed through the on-shell $NN$ amplitudes ($pp$ amplitude $M_p$ and $pn$ amplitude $M_n$) and the deuteron wave function $\Psi_d$:

$$M(\mathbf{q}) = M^{(s)}(\mathbf{q}) + M^{(d)}(\mathbf{q}), \tag{2}$$

$$M^{(s)}(\mathbf{q}) = \int \mathrm{d}^3 r\, e^{i\mathbf{qr}/2}\Psi_d(\mathbf{r})\left[M_n(\mathbf{q}) + M_p(\mathbf{q})\right]\Psi_d(\mathbf{r}), \tag{3}$$

$$M^{(d)}(\mathbf{q}) = \frac{i}{4\pi^{3/2}}\int \mathrm{d}^2 q' \int \mathrm{d}^3 r\, e^{i\mathbf{q}'\mathbf{r}}\Psi_d(\mathbf{r})\times \tag{4}$$

$$\Big[M_n(\mathbf{q_2})M_p(\mathbf{q_1}) + M_p(\mathbf{q_2})M_n(\mathbf{q_1}) - M_c(\mathbf{q_2})M_c(\mathbf{q_1})\Big]\Psi_d(\mathbf{r}),$$

where $\mathbf{q}$ is the overall 3-momentum transfer (so that $t = -q^2$ in the centre-of-mass system), while $\mathbf{q_1} = \mathbf{q}/2 - \mathbf{q}'$ and $\mathbf{q_2} = \mathbf{q}/2 + \mathbf{q}'$ are the momenta transferred in collisions with individual target nucleons, and $M_c(\mathbf{q}) = M_n(\mathbf{q}) - M_p(\mathbf{q})$ is the amplitude of the charge-exchange process $pn \to np$.

When spin dependence is taken into account, the $NN$ amplitudes $M_n$, $M_p$ and the deuteron wave function $\Psi_d$ are non-commuting operators in the three-nucleon spin space. They can be expanded into several independent terms that are invariant under spatial rotations and space and time reflections, and the coefficients of the expansions are, respectively, the $NN$ invariant amplitudes (five for both $pp$ and $pn$ scattering) and $S$- and $D$-wave components of the deuteron wave function. The $pd$ amplitude $M$ is also expanded into 12 independent terms. After undertaking some spin algebra and integrating over the spatial coordinate, all the $pd$ invariant amplitudes can be explicitly related to the $NN$ invariant amplitudes and the various components of the deuteron form factor $S(\mathbf{q}) = \int \mathrm{d}^3 r\, e^{i\mathbf{qr}}|\Psi_d(\mathbf{r})|^2$. The detailed derivation and the final formulae of the refined Glauber model can be found in Refs. [10, 11].

The $NN$ invariant amplitudes at low momentum transfers are easily evaluated from the centre-of-mass helicity amplitudes, which can be constructed from empirical $NN$ phase shifts. For the present calculation, we used the phase shifts of the latest PWA solution of the SAID group [13]. There are, in fact, two PWA solutions published in Ref. [13], viz. the unweighted fit SM16 and the weighted fit WF16. Unlike their earlier solution SP07 [12], both new SAID solutions incorporate the recent high-precision COSY-ANKE data [14, 15] on the near-forward differential cross section ($1.0 \leq T_p \leq 2.8$ GeV) and analysing power $A_y$ ($0.8 \leq T_p \leq 2.4$ GeV) in $pp$ elastic scattering and the COSY-WASA data [16] on $A_y$ in $np$ scattering at $T_n = 1.135$ GeV. However, by construction the WF16 solution describes better the new COSY-ANKE results since the weights of these data have here been enhanced.

The $NN$ partial-wave amplitudes obtained in the SM16, WF16 and SP07 solutions begin to deviate significantly from each other only for $T_p \geq 1$ GeV. We examined both new PWA solutions at $T_p = 900$ MeV and found the $pd$ differential cross section with WF16 input to be lower than that produced by SM16 by between 1% and 3% for $0.08 < |t| < 0.26$ (GeV/$c$)$^2$. This small difference is some measure of the uncertainties arising from the input on-shell $NN$ amplitudes.

For three other energies ($T_p = 800$, 950 and 1000 MeV) we employed the WF16 $NN$ PWA solution and at $T_p = 1$ GeV we also compared the results with those obtained with the SP07 input used in earlier works [10, 11]. The changes ranged from 1% to 8% in the momentum transfer interval $0.08 < |t| < 0.26$ (GeV/$c$)$^2$.

Due to the rapid fall-off of the $NN$ amplitudes with momentum transfer, the $pd$ predictions in the Glauber model are sensitive mainly to the long-range behaviour of the deuteron wave function. We used the one derived from the CD-Bonn $NN$-potential model [21] but choosing a different (but realistic) wave function would change the resulting $pd$ cross section by not more than about 1–2% [11].

The dependence of the $NN$ helicity amplitudes on the momentum transfer $q$, as well as the dependence of the deuteron $S$- and $D$-wave functions on the inter-nucleon distance $r$, were parameterised by convenient five-Gaussian fits [10, 11]. The fitted $NN$ amplitudes coincide with exact ones at momentum transfers $q < 0.7$ GeV/$c$ and the deuteron wave functions at distances $r < 20$ fm. This parametrisation allows us to perform the calculations fully analytically.

## 5. Results

The normalisation of the data presented here is obtained using the fit

$$\mathrm{d}\sigma/\mathrm{d}t = \exp(a + b|t| + c|t|^2)\ \mu\mathrm{b}/(\mathrm{GeV}/c)^2 \tag{5}$$

in the momentum transfer range $0.05 < |t| < 0.4$ (GeV/$c$)$^2$ to the combined database from Refs. [4, 5, 6, 7, 8], which led to the parameters $a = 12.45$, $b = -27.24$ (GeV/$c$)$^{-2}$ and $c = 26.31$ (GeV/$c$)$^{-4}$. To normalise the acceptance-corrected counts at each beam momentum, both the fit to the reference database as well as the numbers of counts are integrated over the momentum transfer range $0.08 < |t| < 0.09$ (GeV/$c$)$^2$. Assuming $\mathrm{d}\sigma/\mathrm{d}t$ is independent of the beam momentum, the ratio between the two integrals defines the scaling factor for each beam momentum that takes into account, e.g., different integrated luminosities. The differential cross sections thus determined for all 16 beam momenta are shown in Fig. 4.

The plots of differential cross sections at the 16 different beam momenta shows that their shapes are independent of beam momentum over the available momentum range. As a consequence, it is possible to evaluate the differential cross section for each of the 18 momentum transfer bins averaged over the 16 energies (cf. Fig. 4, Fig. 5, and Table 2). The systematic uncertainties caused by, e.g., the uncertainty in the angle calibration in the D2 magnet are negligible compared to the statistical uncertainties that are presented in Table 2.

Table 2: Differential cross section $\overline{\mathrm{d}\sigma/\mathrm{d}t}$ and statistical uncertainty of $dp$ elastic scattering averaged over all 16 different beam momenta.

| $\|t\|$ (GeV/$c$)$^2$ | $\overline{\mathrm{d}\sigma/\mathrm{d}t}$ $\mu$b/(GeV/$c$)$^2$ | $\Delta\overline{\mathrm{d}\sigma/\mathrm{d}t}_{\mathrm{stat}}$ $\mu$b/(GeV/$c$)$^2$ |
|---|---|---|
| 0.085 | 29898 | 193 |
| 0.095 | 23624 | 155 |
| 0.105 | 21014 | 140 |
| 0.115 | 16448 | 112 |
| 0.125 | 13562 | 95 |
| 0.135 | 11295 | 82 |
| 0.145 | 8546 | 65 |
| 0.155 | 7534 | 59 |
| 0.165 | 6212 | 51 |
| 0.175 | 5098 | 45 |
| 0.185 | 4264 | 39 |
| 0.195 | 3575 | 35 |
| 0.205 | 2963 | 31 |
| 0.215 | 2573 | 29 |
| 0.225 | 2249 | 26 |
| 0.235 | 1909 | 24 |
| 0.245 | 1575 | 21 |
| 0.255 | 1379 | 20 |

From the comparison of the results with the theoretical calculation at $T_p = 900$ MeV (see Figs. 4 and 5), it is seen that the refined Glauber model describes our data very well at low momentum transfers $0.08 < |t| < 0.2$ (GeV/$c$)$^2$. It is also evident from Fig. 5 that the refined Glauber model calculation agrees similarly with the existing database for $|t| < 0.1$ (GeV/$c$)$^2$. Fig. 6 shows the ratio of the averaged cross section determined in the present experiment to that calculated within the refined Glauber model. The scatter of this ratio around unity for $0.08 < |t| < 0.18$ (GeV/$c$)$^2$ is consistent with the scatter of experimental data around the smooth curve fitting the reference database (see Fig. 6).

At the higher momentum transfers, the theoretical curve begins to deviate from experiment and this is likely to be due to a failure of the small-momentum-transfer approximations (account of only single and double scattering, neglect of recoil, etc.) involved in the Glauber theory. On the other hand, it was found in Ref. [10] that at the lower energies of $T_p = 250$ and 440 MeV the refined Glauber model calculations agree with the data on $pd$ elastic differential cross section out to at least $|t| = 0.3$ (GeV/$c$)$^2$, i.e., in the same region where exact three-body Faddeev equations describe the data. However, the accuracy of the Glauber model, which is a high-energy approximation to the exact theory, should get better at higher collision energy.

The deviations noted here for $|t| > 0.2$ (GeV/$c$)$^2$ might arise from dynamical mechanisms that are not taken into account in either the approximate (Glauber-like) or the exact (Faddeev-type) approach. For example, there could be

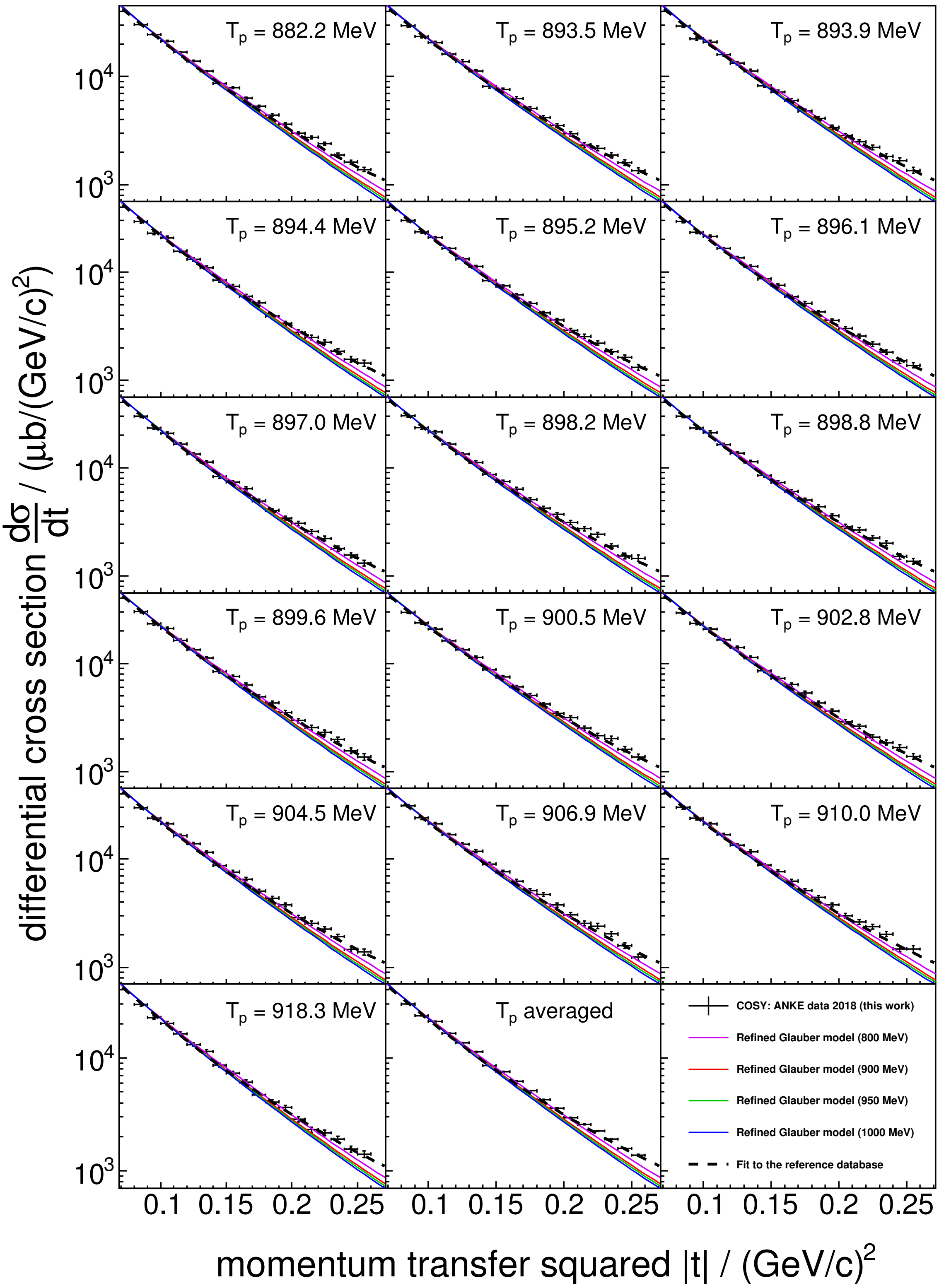


Figure 4: Differential cross sections for deuteron-proton elastic scattering for deuteron laboratory momenta between 3120.17 and 3204.16 MeV/$c$. These are labeled in terms of the proton kinetic energy for a deuteron target ($882.2 \leq T_p \leq 918.3$ MeV). Also shown is the average over the 16 available measurements. The purple ($T_p = 800$ MeV), red ($T_p = 900$ MeV), green ($T_p = 950$ MeV), and blue ($T_p = 1000$ MeV) lines represent the refined Glauber model calculations (with the use of the SAID $NN$ PWA, solution WF16 [13]) and the dashed black line the fit to the $dp$-elastic database from [4, 5, 6, 7, 8].

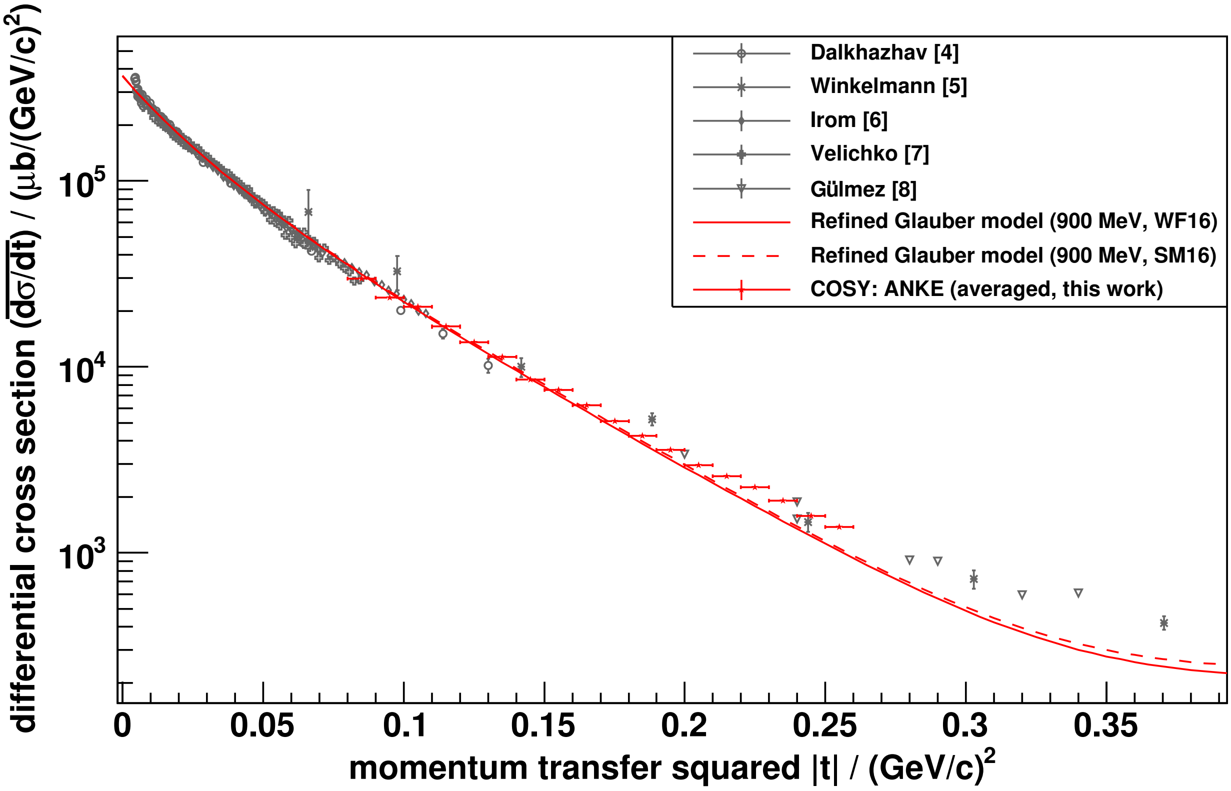


Figure 5: Differential cross sections $\overline{d\sigma/dt}$ averaged over the available 16 energies between 882.2 MeV $\leq T_p \leq$ 918.3 MeV compared with the existing database [4, 5, 6, 7, 8] and the refined Glauber model calculation at $T_p = 900$ MeV (with the use of the SAID $NN$ PWA, solutions WF16 and SM16 [13]).

contributions from a three-nucleon ($3N$) force whose importance rises with collision energy and momentum transfer. One conventional $3N$-force, induced by two-pion exchange with an intermediate $\Delta(1232)$-isobar excitation, is known to contribute to *pd* large-angle scattering at intermediate energies (see, e.g., [22]). However, one might also consider three-body forces caused by the meson exchange between the proton and the six-quark core of the deuteron (the deuteron dibaryon) [23]. Indeed, at larger momentum transfers, the incident proton probes shorter $NN$ distances in the deuteron, so that, the proton scattering off the deuteron as a whole could occur with increasing probability. The preliminary results of taking the one-meson-exchange between the incident proton and deuteron dibaryon into account in *pd* elastic scattering have shown this $3N$-force contribution to increase slightly the *pd* differential cross section already at moderate momentum transfers [24]. This interesting question clearly requires further investigation.

The calculations at different proton energies from 800 to 1000 MeV show a gradual energy dependence of the *pd* differential cross section (see Fig. 4). The theoretical curves at four energies intersect at around $|t| = 0.08$ (GeV/$c$)$^2$ and then begin to deviate from each other. The difference between the calculated cross sections at $T_p = 800$ and 1000

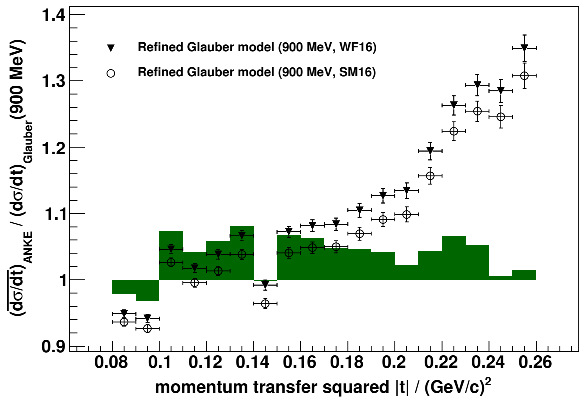


Figure 6: Ratio of our measured differential cross sections $\overline{d\sigma/dt}$ averaged over the available 16 energies to the refined Glauber model calculation at $T_p = 900$ MeV (with the use of the SAID $NN$ PWA, solutions WF16 and SM16 [13]). The green bars represent the ratio of the averaged differential cross sections to the fit to the reference database.

MeV reaches 13% at $|t| = 0.2$ (GeV/$c$)$^2$. The increasing slope of the curve implies that at these energies the interaction radius in $pd$ (as well as $NN$) elastic scattering effectively increases with energy. As a result, the forward diffraction peak in the cross section becomes higher and narrower. This means that the $pd$ elastic cross section integrated over $0 < |t| < 0.2$ (GeV/$c$)$^2$ increases slightly with energy (by 4% from 800 to 1000 MeV), though its part taken from $|t| = 0.08$ (GeV/$c$)$^2$ (the lower limit of the present experiment) decreases a little. Hence, whereas the $pd$ elastic cross section as a function of the momentum transfer squared is usually assumed to be constant in the energy and momentum-transfer range considered, the present model calculations reveal a slight energy dependence of the magnitude and slope of the $pd$ elastic cross section. This result has already been taken into account for normalisation of the recent COSY-WASA experimental data on the $\eta$-meson production in $pd$ collisions [25].

## 6. Summary

Due to its small number of active particles, deuteron-proton elastic scattering at intermediate energies is well suited for the study of various non-standard mechanisms of hadron interaction, such as the production of nucleon isobars, dibaryon resonances, etc. However, even for $dp$ elastic scattering, the experimental database is scarce at momentum transfers $|t| > 0.1$ (GeV/$c$)$^2$. In this work, new precise measurements of the differential cross sections for $dp$ elastic scattering at 16 equivalent proton energies between $T_p = 882.2$ MeV and $T_p = 918.3$ MeV in the range $0.08 < |t| < 0.26$ (GeV/$c$)$^2$ have been presented. Since the shapes of the differential cross sections were found to be independent of beam momentum, it was possible to determine precise average values over the whole momentum transfer range.

The experimental data at low momentum transfers $|t| < 0.2$ (GeV/$c$)$^2$ are well described by the refined Glauber approach at an average energy $T_p = 900$ MeV. These calculations take full account of spin degrees of freedom and use accurate input $NN$ amplitudes based on the most recent partial-wave analysis of the SAID group [13]. The deviations of the theoretical predictions from experimental data observed at the higher momentum transfers are likely to be due to failure of the small-momentum-transfer approximations involved in the Glauber model. These deviations might also reflect the missing contributions of some dynamical mechanisms such as $3N$ forces.

The calculations at different energies, i.e., $T_p = 800$, 900, 950 and 1000 MeV, show a slight energy dependence (increasing slope) in the $pd$ elastic cross section as a function of momentum transfer squared $|t|$. The predicted energy dependence may be trusted in the momentum transfer region where the refined Glauber model describes the data. This behaviour should be taken into account when using $pd$ elastic scattering for the normalisation of other data. However, the energy dependence found in this region is so weak that it cannot be identified in existing data. Very precise measurements for at least two distinct energies (say, $T_p = 800$ and 1000 MeV) would be needed to observe it.

In addition to the unpolarised differential cross sections, it would be interesting to study the momentum transfer and energy behaviour of polarisation observables (analysing powers, etc.), which can readily be calculated within the refined Glauber model at the same energies $T_p = 800$–1000 MeV. The theoretical predictions for such observables will be presented in a forthcoming paper.

## Acknowledgments

We are grateful to other members of the ANKE collaboration and the COSY crew for their work and the good experimental conditions during the beam time. This work has been supported by the JCHP FEE and Russian Foundation for Basic Research, grant No. 16-02-00265.

## References

[1] T. Mersmann, et al., Phys. Rev. Lett. 98 (2007) 242301. doi:10.1103/PhysRevLett.98.242301. arXiv:nucl-ex/0701072.

[2] T. Rausmann, et al., Phys. Rev. C80 (2009) 017001. doi:10.1103/PhysRevC.80.017001. arXiv:0905.4595.

[3] M. Mielke, et al., Eur. Phys. J. A50 (2014) 102. doi:10.1140/epja/i2014-14102-2. arXiv:1404.2066.

[4] N. Dalkhazhav, et al., Sov. J. Nucl. Phys. 8 (1969) 196–202. [Yad. Fiz. 8 (1968), 342].

[5] E. Winkelmann, et al., Phys. Rev. C21 (1980) 2535–2541. doi:10.1103/PhysRevC.21.2535.

[6] F. Irom, et al., Phys. Rev. C28 (1983) 2380–2385. doi:10.1103/PhysRevC.28.2380.

[7] G. N. Velichko, et al., Sov. J. Nucl. Phys. 47 (1988) 755–759. [Yad. Fiz.47,1185(1988)].

[8] E. Guelmez, et al., Phys. Rev. C43 (1991) 2067–2076. doi:10.1103/PhysRevC.43.2067.

[9] V. Franco, R. J. Glauber, Phys. Rev. 142 (1966) 1195–1214. doi:10.1103/PhysRev.142.1195.

[10] M. N. Platonova, V. I. Kukulin, Phys. Rev. C81 (2010) 014004. doi:10.1103/PhysRevC.81.014004,10.1103/PhysRevC.94.069902. arXiv:1612.08694, [Erratum: Phys. Rev.C94,no.6,069902(2016)].

[11] M. N. Platonova, V. I. Kukulin, Phys. Atom. Nucl. 73 (2010) 86–106. doi:10.1134/S1063778810010114, [Yad. Fiz.73,90(2010)].

[12] R. A. Arndt, W. J. Briscoe, I. I. Strakovsky, R. L. Workman, Phys. Rev. C76 (2007) 025209. doi:10.1103/PhysRevC.76.025209. arXiv:0706.2195.

[13] R. L. Workman, W. J. Briscoe, I. I. Strakovsky, Phys. Rev. C94 (2016) 065203. doi:10.1103/PhysRevC.94.065203. arXiv:1609.01741.

[14] D. Mchedlishvili, et al., Phys. Lett. B755 (2016) 92–96. doi:10.1016/j.physletb.2016.01.066. arXiv:1510.06162.

[15] Z. Bagdasarian, et al., Phys. Lett. B739 (2014) 152–156. doi:10.1016/j.physletb.2014.10.054. arXiv:1409.8445.

[16] P. Adlarson, et al. (WASA-at-COSY), Phys. Rev. Lett. 112 (2014) 202301. doi:10.1103/PhysRevLett.112.202301. arXiv:1402.6844.

[17] S. Barsov, et al. (ANKE), Nucl. Instrum. Meth. A462 (2001) 364–381. doi:10.1016/S0168-9002(00)01147-5.

[18] A. Khoukaz, et al., Eur. Phys. J. D5 (1999) 275.

[19] P. Goslawski, et al., Phys. Rev. D85 (2012) 112011. doi:10.1103/PhysRevD.85.112011. arXiv:1204.3520.
[20] P. Goslawski, et al., Phys. Rev. ST Accel. Beams 13 (2010) 022803. doi:10.1103/PhysRevSTAB.13.022803. arXiv:0908.3103.
[21] R. Machleidt, Phys. Rev. C63 (2001) 024001. doi:10.1103/PhysRevC.63.024001. arXiv:nucl-th/0006014.
[22] K. Sekiguchi, et al., Phys. Rev. C89 (2014) 064007. doi:10.1103/PhysRevC.89.064007.
[23] V. I. Kukulin, V. N. Pomerantsev, M. Kaskulov, A. Faessler, J. Phys. G30 (2004) 287–308. doi:10.1088/0954-3899/30/3/005. arXiv:nucl-th/0308059.
[24] M. N. Platonova, V. I. Kukulin, J. Phys. Conf. Ser. 381 (2012) 012110. doi:10.1088/1742-6596/381/1/012110.
[25] P. Adlarson, et al. (WASA-at-COSY) (2018). arXiv:1801.06671.